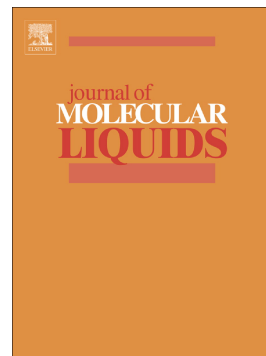


Journal Pre-proof

Polarization effect in luminescent mesogenic BF₂ complexes derived from heterocyclic benzothiazoles

Yuan-Chun Hsu, Chun-Yang Wang, Pei-Chi Hsiao, Yi-Hong Cai, Gene-Hsiang Lee, Chung K. Lai



PII: S0167-7322(19)32889-2

DOI: <https://doi.org/10.1016/j.molliq.2019.111660>

Reference: MOLLIQ 111660

To appear in: *Journal of Molecular Liquids*

Received date: 22 May 2019

Revised date: 24 August 2019

Accepted date: 28 August 2019

Please cite this article as: Y.-C. Hsu, C.-Y. Wang, P.-C. Hsiao, et al., Polarization effect in luminescent mesogenic BF₂ complexes derived from heterocyclic benzothiazoles, *Journal of Molecular Liquids*(2019), <https://doi.org/10.1016/j.molliq.2019.111660>

This is a PDF file of an article that has undergone enhancements after acceptance, such as the addition of a cover page and metadata, and formatting for readability, but it is not yet the definitive version of record. This version will undergo additional copyediting, typesetting and review before it is published in its final form, but we are providing this version to give early visibility of the article. Please note that, during the production process, errors may be discovered which could affect the content, and all legal disclaimers that apply to the journal pertain.

© 2019 Published by Elsevier.

Polarization effect in luminescent mesogenic BF₂ complexes derived from heterocyclic benzothiazoles

Yuan–Chun Hsu ^a, Chun–Yang Wang ^a, Pei–Chi Hsiao ^a, Yi–Hong Cai ^a,
Gene–Hsiang Lee ^b, Chung K. Lai ^{a*}

^a *Department of Chemistry, National Central University, Chung–Li 32001, Taiwan, ROC*

^b *Instrumentation Center, National Taiwan University, Taipei 10660, Taiwan, ROC*

ABSTRACT

Two series of benzo(thia)xazoles **1-2** and one series of boron difluoride complexes **2-BF₂** derived from benzothiazoles **2** were reported, and their mesomorphic and optical properties were investigated. The crystal and molecular structures of compound **2** and **2-BF₂** (all n = 8) were determined by means of X–ray structural analysis, and both crystallize in the triclinic P-1 and monoclinic P2₁/c. The geometry at boron center is perfectly tetrahedral, and the overall molecular shapes are considered as rod–shape. Both benzo(thia)xazoles **1** and **2** exhibited N or/and SmC phase, and boron complexes **2-BF₂** formed N or/and SmC phase. Benzothiazoles **2** showed a much wider temperature range of mesophase than those of benzoxazoles **1**, which were attributed to the better polarization by sulfur atom incorporated. Boron complexes **2-BF₂** (n = 10, 12) emitted a yellow–to–green emission at $\lambda_{\text{max}} = 569\text{--}571$ nm in CH₂Cl₂. This is the first mesogenic BF₂ complexes derived from benzothiazoles.

* Corresponding author

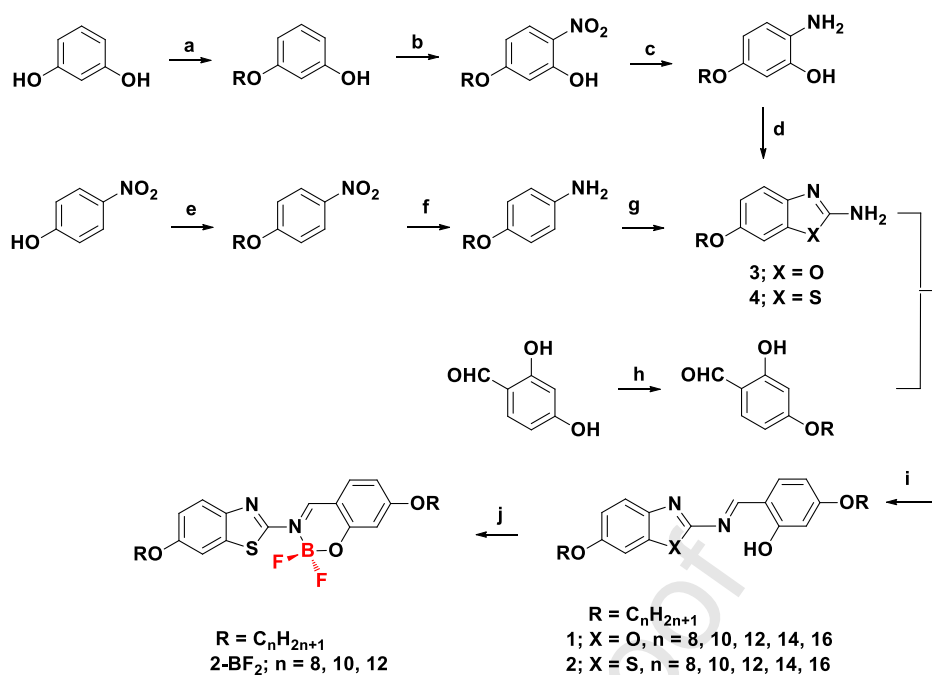
E-mail address: cklai@cc.ncu.edu.tw

1. Introduction

The research on boron difluoride (BF_2) complexes [1-4] incorporating organic π -conjugated backbones or motifs have extensively continuing during the past decades; many unique complexes were prepared and investigated in a variety of applications. Light-emissive materials [5-7] were among the most widely areas of molecular materials due to their unique, tunable and useful absorption and emission properties. By designing appropriate chelating ligands, the molecular structures of BF_2 complexes could be modified or tuned for the optical properties. Boron difluoride often coordinates oxygen or/and nitrogen atoms with chelating ligands and the resulting boron complexes with a coordination number of four ($\text{CN} = 4$) and a tetrahedral geometry were often obtained. On the other hand, among these known BF_2 complexes, three coordination modes of $[\text{F}_2\text{B}-\text{O},\text{O}]$ [6-11], $[\text{F}_2\text{B}-\text{O},\text{N}]$ [12-16] and $[\text{F}_2\text{B}-\text{N},\text{N}]$ [17-21] were often generated. The common chelating ligands incorporated to form BF_2 complexes as the core structures included β -diketonates, ketoiminates and diiminates. Many mesogenic momo- BF_2 [22-25], mesogenic bis(BF_2)₂ [26-28] or nonmesogenic tris(BF_2)₃ [29-30] complexes were consequently obtained. Boron diketonates were not only investigated for liquid crystalline materials, but also to work as building blocks for luminogenic nanomaterials. A typical emission band between $\lambda_{\text{max}} = 450\text{-}650$ nm was often observed. Furthermore, several boron β -diketonate complexes [31] exhibited a mechanofluouochromic (MFC) behavior. In contrast, boron complexes of diiminates and benzothiazoxoles [32-34] have been showed to be a potential candidate for use as aggregation-induced-emission (AIE) [35-39] materials; diiminate derivatives were easily obtained by replacing a more electronegative nitrogen atom from diketonates. Recently, the use of heterocyclic chelating ligands, such as pyrazoles [40-42] and benzoxazoles [43] as building blocks has been widely applied in their structural modifications, as well as their potential applications. A few luminescent di- and trinuclear boron complexes derived from iminopyrrolyl spacer ligands [44] were demonstrated in the use of OLEDs. The use of benzothiazoles in the biological activities [45-46] has also been reviewed.

2.1 Synthesis and Characterization

The synthetic pathways to boron difluoride complexes **2-BF₂** are summarized in Scheme 1. The experimental preparations of compounds **2** were followed by our previous procedures. The compounds **1** were obtained by the reactions of 6-alkoxybenzo [d]oxazol-2-amines and 4-alkoxy-2-hydroxybenzaldehydes in refluxing absolute ethyl alcohol for 8 h. On the other hands, the compounds **2**, (E)-5-alkoxy-2-(((6-(dodecyloxy)benzo[d]thiazol-2-yl)imino)methyl)phenol were obtained by the reaction of 6-alkoxybenzo[d] thiazol-2-amines and 4-alkoxy-2-hydroxy benzaldehydes in refluxing absolute ethyl alcohol for 8 h. All compounds **1** and **2** were isolated as light yellow solids. The final boron complexes **2-BF₂** were obtained by the reactions of (E)-5-alkoxy-2-(((6-alkoxybenzo[d]thiazol-2-yl)imino)methyl)phenols and boron trifluoride diethyl etherate in refluxing in CH₂Cl₂ for 1.5 h. The complexes **2-BF₂** isolated as orange powders were purified by column chromatography eluting with CH₂Cl₂. These boron complexes are very air stable and soluble in most organic solvents. However, the similar reactions of benzoxazoles **1** and boron trifluoride diethyl etherate in refluxing in CH₂Cl₂ gave no BF₂ complexes; a small amount of starting materials were recovered. The ¹H, ¹³C NMR and ¹⁹F NMR spectroscopy were used to characterize all intermediates, and the elemental analysis and HRMS were used to confirm the purity of the boron complexes. For example, the ¹H NMR data in CDCl₃, showed two characteristic peaks assigned to phenolic-H (-COH) and methanimine-H (-CH=N), summarized in Table 1. On the ¹H NMR spectra, the original singlet assigned for phenolic-OH of compounds **2** at δ 12.63–12.64 were all disappeared upon coordination to BF₂ moiety. On the ¹⁹F NMR spectra, a doublet of doublets appeared at δ -133.45 to -133.48 (i.e. ¹⁰B-F, 0.2F) and ~ -133.53to -133.55 (i.e. ¹¹B-F, 0.8F) was observed for compounds **2-BF₂**. Elemental analysis and mass were also used to confirm the purity of the boron complexes.



Scheme 1. Reactions and Reagents. (a) $C_nH_{2n+1}Br$ (1.5 eq), $KHCO_3$ (3.0 eq), KI (0.6 eq), refluxing in acetone, 48 h, 58-63%. (b) $NaNO_2$, HNO_3 , CH_2Cl_2 , 0 °C, 8 h, 25-29%. (c) 10% Pd/C, refluxing in EtOH, 4 h, 81-86%. (d) $BrCN$ (7.0 eq), MeOH, rt, 4 d, 70-78%. (e) $C_nH_{2n+1}Br$ (1.5 eq), K_2CO_3 (3.0 eq), KI (0.6 eq), refluxing in acetone, 24 h, 87-92%. (f) 10% Pd/C, refluxing in EtOH, 4 h, 83-88%. (g) $KSCN$ (2.0 eq), Br_2 (1.0 eq), rt, 8 h, 40-46%. (h) $C_nH_{2n+1}Br$ (1.5 eq), $KHCO_3$ (3.0 eq), KI (0.6 eq), refluxing in acetone, 48 h, 40-80%. (i) Refluxing in dry EtOH, 8 h, , 78-82%. (j) Boron trifluoride diethyl etherate (2.0 eq.), refluxed in CH_2Cl_2 , 2 h, 25-30%.

Table 1

The characteristic 1H NMR peaks^a assigned for compounds **1-2** and **2-BF₂**.

Compd.	1	2	2-BF₂
-OCH ₂	3.96–4.03 (m)	3.98–3.99 (t)	4.00 (t), 4.05–4.06 (t)
-CH=N	9.21–9.22 (s)	9.02–9.04 (br)	9.35–9.36 (br)
-COH (phenolic)	12.60 (s)	12.63–12.64 (br)	–

^a solution in $CDCl_3$; unit (δ) in ppm; s = singlet, t = triplet, m = multiplet and br = broad.

2.2 Single structure and molecular structures of (*E*)-5-(octyloxy)-2-(((6-(octyloxy)benzo[*d*]thiazol-2-yl)imino)methyl)phenol **2** ($n = 8$) and boron complex of 7-(octyloxy)-3-(6-(octyloxy)benzo[*d*]thiazol-2-yl)-2,2-difluoro-2*H*-benzo[*e*] [1,3,2]oxazaborinin-3-ium- 2-uide **2-BF₂** ($n = 8$).

In order to understand the correlation between the molecular structures and the formation of mesophases, two single crystals of pale yellow compound **2** ($n = 8$) and its orange boron complex **2-BF₂** ($n = 8$) were obtained and their single crystallographic data were investigated. Two crystals suitable for X-ray diffraction analysis were slowly grown from THF at room temperature. **Fig. 1** shows the molecular structures with the atomic numberings, and Table 2 lists the crystallographic and structural refinement data for the two compounds. The crystal **2** crystallizes in triclinic space group P-1, with $a = 6.7094(3) \text{ \AA}$, $b = 14.2811(7) \text{ \AA}$, $c = 16.1874(8) \text{ \AA}$, and $Z = 2$, in contrast, the crystal **2-BF₂** crystallizes in monoclinic space group P2₁/c, with $a = 16.5816(4) \text{ \AA}$, $b = 10.8598(3) \text{ \AA}$, $c = 17.0697(4) \text{ \AA}$, and $Z = 4$. The bond length of $d = 1.294 \text{ \AA}$ for imine $-\text{CH}=\text{N}$ (i.e. atom C1–N1) in crystal **2** increased to $d = 1.334 \text{ \AA}$ upon coordination to boron atom in crystal **2-BF₂** (see Table 3). The four angles at tetrahedral boron atom in **2-BF₂** were ranged from $108.9\text{--}111.1^\circ$, slightly derived from perfect 109° (see Table 3). The overall structures of both crystals were considered as rod-like shapes, and the molecular lengths were 33.03 \AA (atom C22–C30 in crystal **2**) and 33.02 \AA (atom C22–C30 in **2-BF₂**). The overall molecular structures in two crystals were quite planar, and the dihedral angles derived from central plane (see **Fig. 2**) to neighboring rings were $\sim 10.05^\circ$ (for **2**) and $\sim 3.899^\circ$ (for **2-BF₂**). The relatively small dihedral angles favored the formation of mesophases.

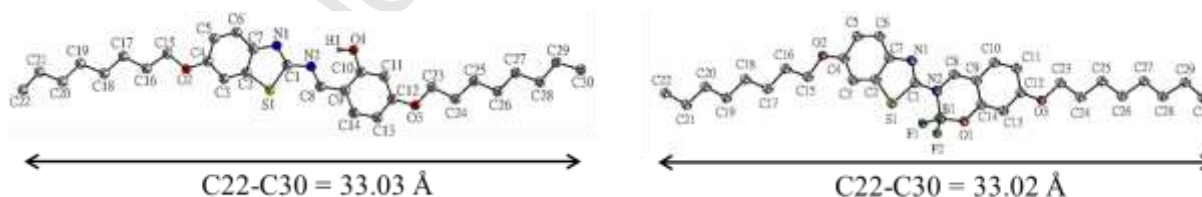


Fig. 1 Two ORTEP drawings for two crystals **2** ($n = 8$, left) and **2-BF₂** ($n = 8$, right) with the numbering schemes, and thermal ellipsoids of non-hydrogen atoms are drawn at the 50% probability level.



Fig. 2 Two dihedral angles between the central boron and neighboring phenyl rings existed in crystals **2** ($n = 8$, left) and **2-BF₂** ($n = 8$, right). P1 and P2 are representative neighboring planes.

Table 2

Crystallographic data for two crystals **2** and **2-BF₂**.

Comps.	2 ($n = 8$)	2-BF₂ ($n = 8$)
Empirical formula	C ₃₀ H ₄₂ N ₂ O ₃ S	C ₃₀ H ₄₁ BF ₂ N ₂ O ₃ S
Formula weight	510.72	558.52
Temperature (K)	150(2)	200(2)
Crystal system	Triclinic	Monoclinic
Space group	P-1	P2 ₁ /c
a (Å)	6.7094(3)	16.5816(4)
b (Å)	14.2811(7)	10.8598(3)
c (Å)	16.1874(8)	17.0697(4)
α (°)	115.115(2)	90
β (°)	94.930(3)	105.7016(12)
γ (°)	94.839(3)	90
Volume (Å ³)	1386.59(11)	2959.09(13)
Z	2	4
Density (calculated, Mg/m ³)	1.223	1.254
Crystal size (mm ³)	0.50 x 0.20 x 0.15	0.359 x 0.247 x 0.027
Theta range for data collection (°)	1.40 to 27.50	4.881 to 71.998
Reflections collected	18918	16793
Independent reflections	6295 [R(int) = 0.0466]	5783 [R(int) = 0.0340]
Final R1, wR2	0.0449, 0.0983	0.0572, 0.1460

Table 3

Selected bond lengths (Å) and angles (°) in crystals **2** and **2-BF₂**.

Crystal 2 ($n = 8$)			
N1–C1	1.294	S1–C1	1.786
C1–N2	1.392	N2–C8	1.294
H1–O1	0.840	O1–C10	1.351
\angle S1–C1–N1	115.92	\angle C1–N2–C8	118.75
\angle S1–C1–N2	121.44	\angle N2–C8–C9	123.11

Crystal **2-BF₂** (n = 8)

N1–C1	1.278	S1–C1	1.751
C1–N2	1.404	N2–C8	1.334
∠ F1–B1–F2	108.9	∠ F1–B1–N2	107.6
∠ N2–B1–O1	109.96	∠ O1–B1–F2	111.1

As expected, a strong intramolecular H–bond was observed in crystal **2**; a distance of ~ 1.934 Å (atom N2...H1) was obtained, as shown **Fig. 3**. In contrast, quite a few weak intermolecular H–bonds were observed in both crystals. A distance of ~ 3.182 Å (atom S1...H1) was obtained for crystal **2**, and a bond length ranged in $d = 2.546 - 2.832$ Å (Table 4) were obtained for crystal **2-BF₂**. The intramolecular H–bonds kept the phenolic ring nearly coplanar to the benzo ring, and the better planar structure was favorable for a better packing both in the solid or/and the liquid crystal state. In contrast, other intermolecular interactions, such as $\sigma-\pi$ or $\pi-\pi$ were also observed in two crystals. In general, the CH... or $\pi-\pi$ interactions were much weaker than H–bonds. A distance ranged from $d = 2.88 - 3.224$ Å were observed in both crystals (Table 5 and **Fig. 4**). These weak intermolecular forces were very crucial on the induction and/or formation of mesophases in such heterocyclic compounds. In crystal lattice, all alkoxy chains were not interdigitated between neighboring molecules; all alkoxy chains were slightly interdigitated, giving a smaller layer distance both in N and SmC phases upon heating to the mesophase temperatures (**Fig. 5**).

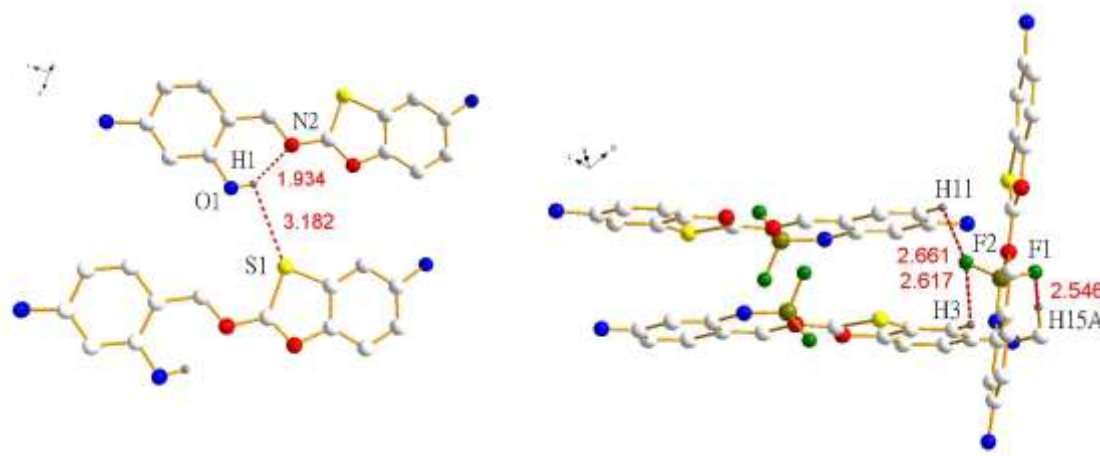
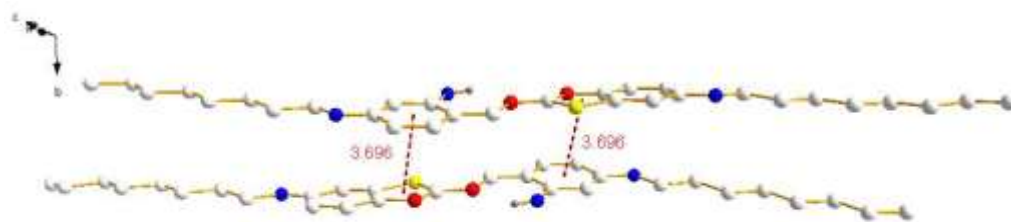


Fig. 3 H-bond interactions observed in crystal **2** (n = 8, left) and **2-BF₂** (n = 8, right).**Table 4**The H-bond interactions observed in crystals **2** and **2-BF₂**.

Comps	H-bonds (D-H...A)	Distances (Å)	Angle D-H...A (°)
Intramolecular H-bond			
2 (n = 8)	N2-H1-O1	1.934	143.7
Intermolecular H-bond			
2-BF₂ (n = 8)	S1-H1-O1	3.182	93.13
	C3-H3-F2	2.661	127.45
	C11-H11-F2	2.617	121.16
	C15-H15A-F1	2.546	138.13
	C25-H25A-F2	2.665	154.69
	C23-H23B-F2	2.832	146.38
	C8-H8-F1	2.648	119.75

Table 5Intermolecular interactions^a observed in crystals **2** and **2-BF₂**.

Comps	σ - π or π - π	Distances (Å)	Angle (ring-H...A) (°)
2 (n = 8)	ring-ring	3.696	–
2-BF₂ (n = 8)	ring-H28B-C28	3.224	145.84
	ring-H26B-C26	2.998	134.43
	ring-H23B-C23	2.880	135.31

^a: measured from the center of ring to the atom.

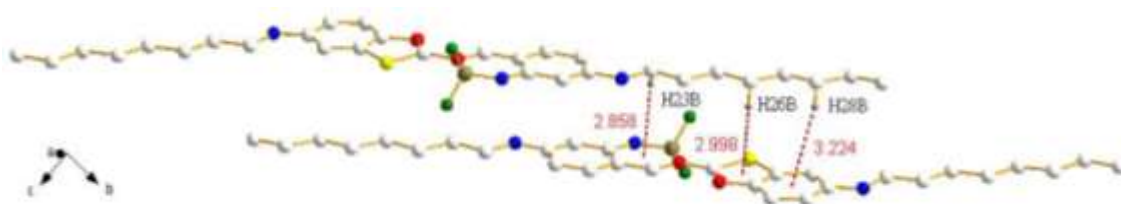


Fig. 4 The π - π interactions observed in crystals **2** ($n = 8$, top) and **2-BF₂** ($n = 8$, bottom)

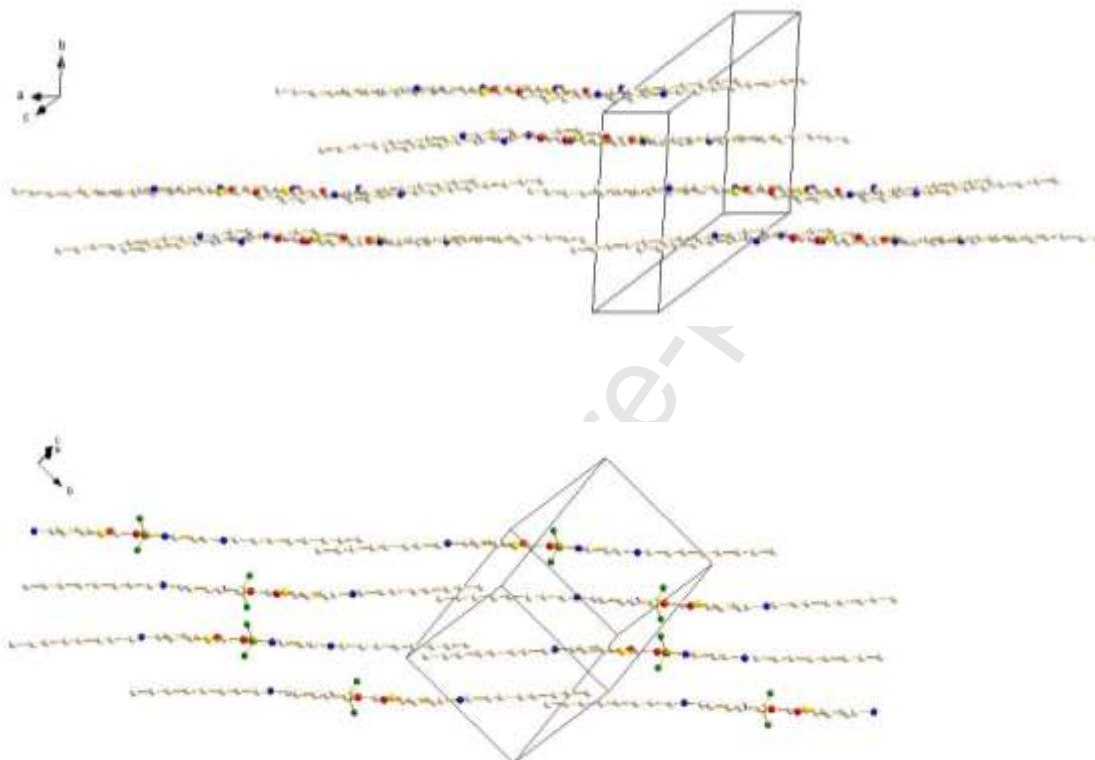


Fig. 5 The layered structures observed in crystal **2** ($n = 8$, top) and **2-BF₂** ($n = 8$, bottom).

2.3 Phase transitions, mesomorphic properties and thermal stability.

The thermal behavior of all compounds **1–2** and **2-BF₂** was studied by polarized optical microscopy and differential scanning calorimetry. The transition temperatures and enthalpies of the compounds **1a–c** and **2-BF₂** are summarized in Table 6. The results showed that all compounds **1–2** formed an enantiotropic mesomorphic behavior. For compounds **1**, all melting temperatures were

ranged from $T_{mp} = 79.4\text{--}97.8$ °C, however, all clearing temperatures increased with the carbon length of the alkoxy chains; $T_{cl} = 93.1$ (n = 8) < 97.1 (n = 10) < 97.6 (n = 12) < 97.7 (n = 14) < 99.9 °C (n = 16), indicating that the van der Waals interaction played an important force in the LC states. All benzoxazole **1** formed N or/and SmC phase; the two derivatives with shorter carbon length (n = 8, 10) formed N phases, and other three derivatives (n = 10, 12, 14, 16) exhibited SmC phase. This is common behavior observed for the rod-like mesogens. Not surprised, the temperature range of mesophases by compounds **1** decreased with carbon length; i.e. $\Delta T = 25.6$ (n = 8) > 21.6 (n = 10) > 14.3 (n = 12) > 9.1 (n = 14) > 4.3 °C (n = 16) on cooling process. The enthalpy changed for the transition of N \rightarrow I phase and SmC \rightarrow I phase was ranged from $\Delta H = 1.39\text{--}1.43$ KJ/mol and 6.67-8.32 KJ/mol. However, the enthalpy for the transition of SmC \rightarrow N phase for compound **1** (n = 10) was often relatively small, i.e. 0.72-0.94 KJ/mol. The mesophases were then first characterized and identified as N and SmC phases by POM; a Schlieren or focal-conics texture was easily observed under POM when cooled from their isotropic states.

Table 6

The phase transitions and enthalpies^[a] of compounds **1-2** and **2-BF₂**.

Comps	Phase transitions and corresponding enthalpies (in parentheses) °C (kJ/mol)	
	The second heating cycle	The second cooling cycle
1; n = 8	Cr 79.4 (31.0) → N 93.1 (1.39) → I	I 92.1 (1.39) → N 66.5 (32.1) → Cr
10	Cr 86.6 (30.4) → SmC 90.8 (0.72) → N 97.1 (1.48) → I	I 92.1 (1.39) → N 89.8 (0.94) → SmC 70.5 (32.3) → Cr
12	Cr 91.0 (50.2) → SmC 97.6 (6.67) → I	I 95.8 (7.57) → SmC 81.5 (54.1) → Cr
14	Cr 93.9 (56.7) → SmC 97.7 (8.32) → I	I 95.8 (7.64) → SmC 86.7 (53.5) → Cr
16	Cr 97.8 ^[b] → SmC 99.9 (76.5) ^[b] → I	I 97.5 (8.93) → SmC 93.2 (63.2) → Cr
2; n = 8	Cr 78.4 (28.1) → SmC 125.9 (2.51) → N 136.6 (2.37) → I	I 135.1 (2.64) → N 124.6 (2.25) → SmC 69.5 (27.7) → Cr
10	Cr 87.1 (0.37) → SmC 136.2 (9.64) → I	I 133.4 (7.91) → SmC 71.4 (30.2) → Cr
12	Cr 89.2 (7.28) → SmC 135.9 (8.61) → I	I 133.1 (9.26) → SmC 76.0 (32.1) → Cr

14	Cr 85.8 (42.3) → SmC 129.4 (12.4) → I	I 128.6 (10.7) → SmC 79.7 (42.2) → Cr
16	Cr 90.0 (47.2) → SmC 125.9 (13.5) → I	I 123.1 (11.6) → SmC 81.5 (49.5) → Cr
2-BF₂ ; n = 8	Cr 116.1 (41.5) → SmC 133.4 (3.69) → N 137.7 (2.83) → I	I 136.1 (2.97) → N 131.1 (3.40) → SmC 100.2 (16.5) → Cr
10	Cr 117.0 (20.0) → SmC 142.9 (8.97) → I	I 141.1 (8.42) → SmC 96.7 (23.7) → Cr
12	Cr 111.0 (29.0) → SmC 145.8 (11.5) → I	I 143.9 (11.0) → SmC 94.9 (32.3) → Cr

[a]: n = the carbon numbers of alkoxy chains; Cr = crystal, SmC = smectic C, N = nematic and I = isotropic phases.

[b]: observed from POM due to overlapping with clearing peak

In contrast, all benzothiazoles **2** exhibited an improved mesomorphic behavior over benzoxazoles **1**. Both compounds **1** and **2** are structurally similar, however, benzothiazole **2** has a sulfur atom incorporated, larger in size than that of oxygen in benzoxazoles **1** (i.e. covalent radii $1.02 \times 10^{-10} > 0.73 \times 10^{-10}$ m). The difference in the clearing temperature might be attributed to the molecular size or/and polarization effect. The clearing temperature of benzothiazoles **2** also decreased with carbon length of alkoxy chains; i.e. $T_{cl} = 136.6$ (n = 8) > 136.2 (n = 10) > 135.9 (n = 12) > 129.4 (n = 14) > 125.4 °C (n = 16), which were relatively higher than those of benzoxazoles **1** by an $\Delta T_{cl} = 43.5$ (n = 8) > 39.1 (n = 10) > 38.3 (n = 12) 31.7 (n = 14) > 26.0 °C (n = 16). In addition, the temperature range of mesophases also decreased with carbon length; i.e. $\Delta T_{meso} = 65.6$ (n = 8) > 62.0 (n = 10) > 57.1 (n = 12) > 48.9 (n = 14) > 41.6 C (n = 16) °C on the cooling process. All benzoxazole **2** formed N or/and SmC phase; the derivatives with n = 8 formed N phases, and all other derivatives (n = 10, 12, 14, 16) exhibited SmC phase. The mesophases were also characterized and identified as N and SmC phases by POM; they showed identical textures as compounds **1**; a Schlieren and focal-conic texture for N and SmC phases was observed when cooled from their isotropic states (**Fig. 6**). The N or SmA phase, but not SmC phase showed homeotropic behavior under polarized microscope. Also, the Schlieren textures observed by SmC phases gave only singularities with four brushes while N phases showed extra singularities with two brushes. The much wider temperature of mesophase by benzothiazoles **2** was probably attributed to the polarization effect caused by sulfur atom incorporated.

In general, the overall geometries of the complexes are determined or controlled by both the central metal and the organic moiety; a more bulky or steric core might reduce the preferred molecular packing in the solid or LC states. This is particularly true in the design of the metallomesogenic materials when metal was tetrahedral copper, cobalt or zinc ions. However, many such tetrahedral metal complexes and boron-difluoride in this work were demonstrated to be

mesogens when ligands properly designed. Furthermore, the relatively smaller BF_2 moiety might provide a preferred dipole to induce the mesophases. Upon complexation to BF_2 moiety, three complexes **2-BF₂** ($n = 8, 10, 12$) formed enantiotropic N or/and SmC phases. All clearing temperatures were slightly higher than those of compounds **2** by an $\Delta T_{\text{cl}} = 1.1$ ($n = 8$) < 6.7 ($n = 10$) < 10.9 °C ($n = 12$). The results that a slightly increasing in the clearing temperatures and also forming the mesophase were probably attributed to the relatively small steric effect caused by the tetrahedral BF_2 moiety. The temperature range of mesophases increased with carbon length; $\Delta T_{\text{meso}} = 35.9$ ($n = 8$) > 44.4 ($n = 10$) > 49.0 °C ($n = 12$) on the cooling process. The mesophase was identified and characterized as N and SmC phases by POM and XRD experiments. The mesophases were identified and characterized as SmC phase first based on POM. Bar graph showing the phase behavior of compounds **1a–c** was shown in **Fig. 7**.

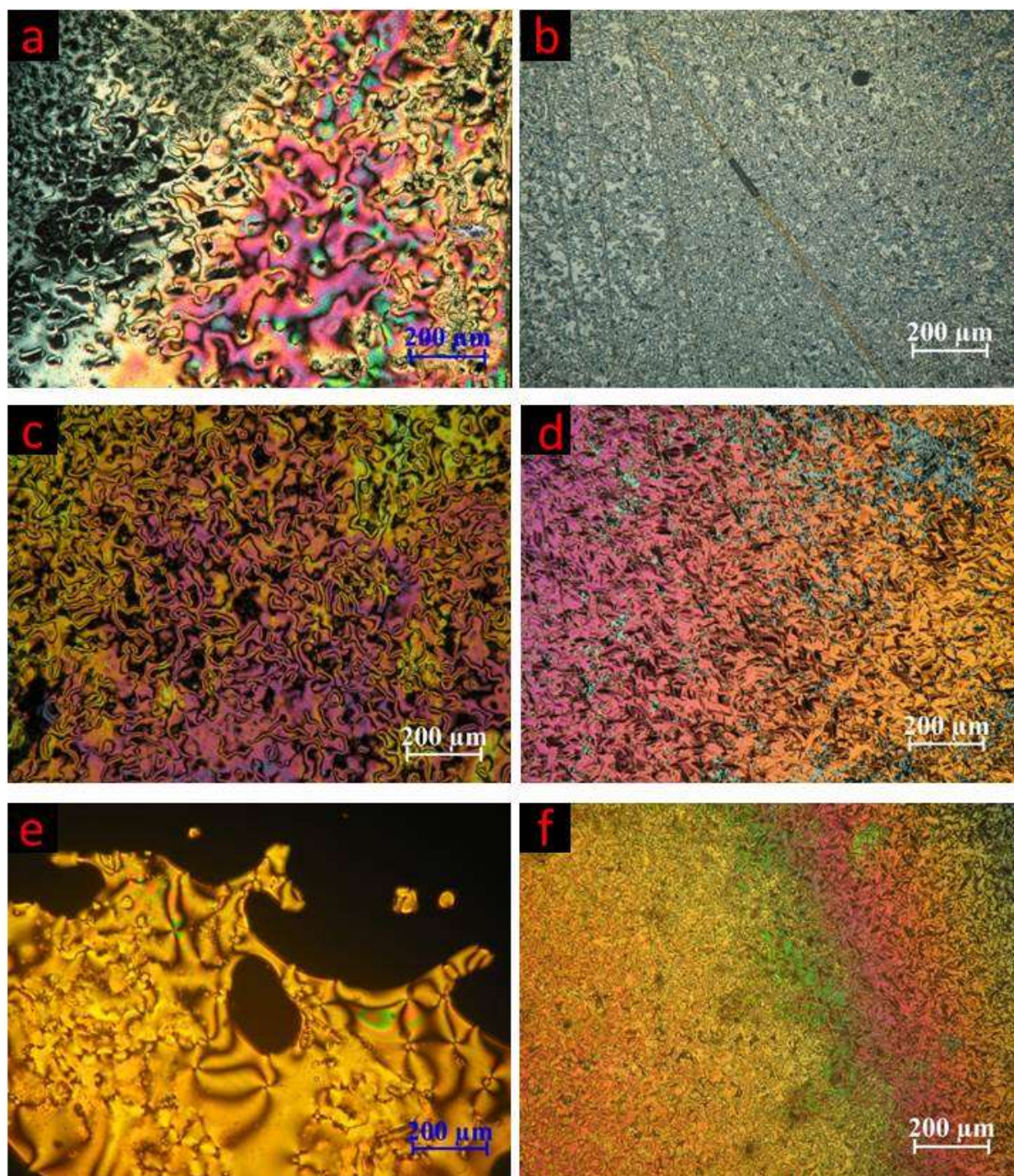


Fig. 6 Optical textures observed. (a) N phase by **1** ($n = 10$) at $92.0\text{ }^{\circ}\text{C}$; (b) SmC phase by **1** ($n = 10$) at $87.0\text{ }^{\circ}\text{C}$; (c) N phase by **2** ($n = 8$) at $130.0\text{ }^{\circ}\text{C}$; (d) SmC phase by **2** ($n = 8$) at $125.0\text{ }^{\circ}\text{C}$; (e) N phase by **2-BF₂** ($n = 8$) at $136.0\text{ }^{\circ}\text{C}$ and (f) SmC phase by **2-BF₂** ($n = 8$) at $122.0\text{ }^{\circ}\text{C}$. All temperatures were taken on cooling process from their isotropic.

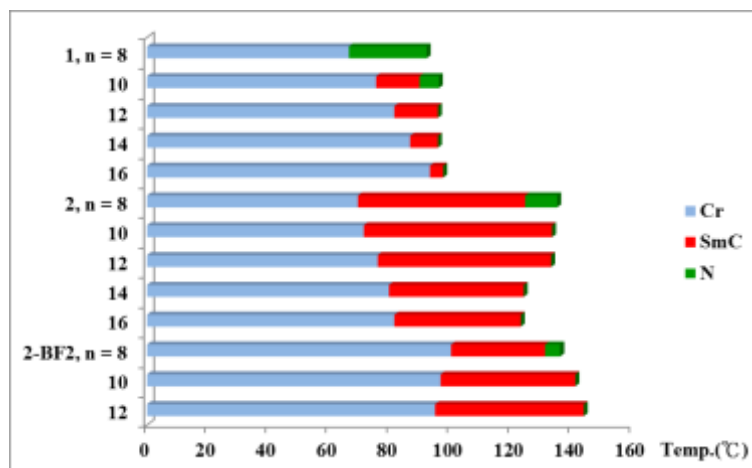


Fig. 7 Bar graphs showing the phase behavior of compounds **1**, **2** and **2-BF₂**.

2.4 Powder X-ray diffractions

Variable-temperature powder XRD diffraction experiments were performed to confirm the structures of the mesophases. **Fig. 8** shows typical diffraction plots for one derivative **2** ($n = 8$) and its boron complex **2-BF₂** ($n = 8$). Both compounds formed similar mesomorphic behavior; SmC phase at lower temperature and N phase at higher temperature due to their similar structures. For compound **2** ($n = 8$) a strong diffraction with a d-spacing of ca. $d = 29.04 \text{ \AA}$ at $138 \text{ }^\circ\text{C}$ and $d = 27.13 \text{ \AA}$ at $125 \text{ }^\circ\text{C}$ was obtained. A relatively broad and weak peak at 29.04 \AA corresponded to N phase; while a sharp and strong at 27.13 \AA corresponded to the SmC phase (Table 8). In N phase the long molecular axes of the individual molecules lie essentially parallel to one another. These d-spacings were slightly larger than those of value (i.e. 33.03 \AA at 150 K) observed from crystallographic data. The long axes of the molecules in SmC phase are tilted with respect to the planes of the layers. The optical character is positive biaxial. The much smaller d-spacing indicated that the molecules were tilted or/and the terminal alkoxy chains were to some extent interdigitated in SmC phase. Furthermore, a very broad and weak peak at $4.53 \sim 4.63 \text{ \AA}$ was observed, and this peak was assigned to the molten alkoxy chains. In contrast, for the compound **2-BF₂** ($n = 8$), a similar XRD plots were observed. a strong diffraction with a d-spacing of ca. $d = 24.87 \text{ \AA}$ at $135 \text{ }^\circ\text{C}$ and $d = 24.12 \text{ \AA}$ at $114 \text{ }^\circ\text{C}$ was obtained. These peaks corresponded to N and SmC phase. Also a very broad and weak peak

at $4.50 \sim 4.55 \text{ \AA}$ was observed, and this peak was assigned to the molten alkoxy chains. A schematic representation of molecular organization proposed in SmA phase by compounds **2** and **2-BF₂** is shown in **Fig. 9** and **Fig. 10**.

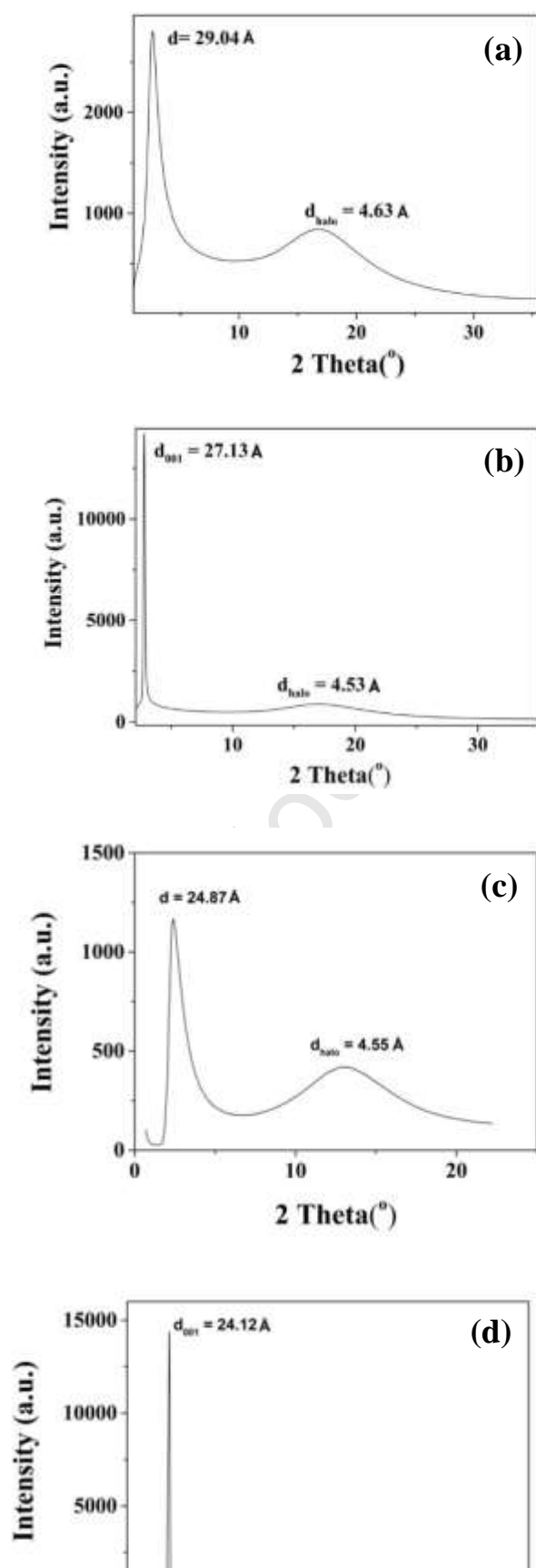


Fig. 8 The powder X-ray diffraction plots. (a) Compound **2** (n = 8) at 138 °C; (b) compound **2** (n = 8) at 125 °C; (c) compound **2-BF₂** (n = 8) at 135 °C and (d) compound **2-BF₂** (n = 8) at 114 °C.

Table 7

The powder X-ray diffraction data for compounds **1-2** and **2-BF₂**.

Compds.	Mesophase/temp. ^a	<i>d</i> -Spacing/Å	ML ^b	Index
1 (n = 8)	N phase at 100 °C	29.67 (29.67)	33.09	
		4.53 (br)		halo
1 (n = 10)	N phase at 95 °C	32.83 (32.83)	38.11	
		4.50 (br)		halo
1 (n = 12)	SmC phase at 105 °C	35.34 (35.34)	43.05	001
		4.52 (br)		halo
1 (n = 14)	SmC phase at 106 °C	37.80 (37.80)	48.37	001
		19.06 (18.90)		002
		4.48 (br)		halo
2 (n = 8)	N phase at 138 °C	29.04 (29.04)	33.03	
		4.63 (br)		halo
	SmC phase at 125 °C	27.13 (27.13)		001
2 (n = 10)	SmC phase at 130 °C	30.54 (30.54)	38.31	001
		4.51 (br)		halo
		34.11 (34.11)		43.27
2 (n = 12)	SmC phase at 100 °C	17.11 (17.06)	48.24	002
		4.53 (br)		halo
		37.64 (37.64)		001
2 (n = 14)	SmC phase at 125 °C	19.06 (18.82)	53.21	002
		4.63 (br)		halo
		39.92 (39.92)		001
2 (n = 16)	SmC phase at 135 °C	19.93 (19.96)	—	002
		4.59 (br)		halo
		24.87 (24.87)		
2-BF₂ (n = 8)	N phase at 135 °C	24.87 (24.87)	—	

	4.55 (br)	halo
SmC phase at 114 °C	24.12 (24.12)	001
	4.50 (br)	halo

^a: Sample was heated above the clearing temperature and the diffraction data recorded on cooling process.

^b: Molecular lengths were calculated by MM2 model.

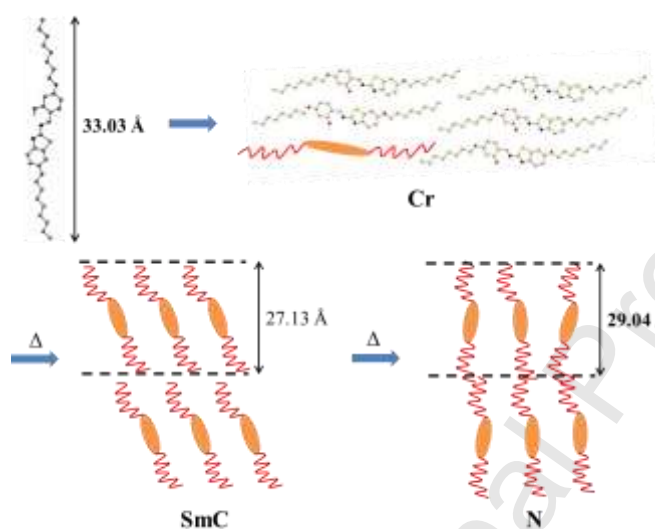


Fig. 9. The molecular arrangements proposed for compound **2** ($n = 8$) in Cr, N and SmC phases. The molecular length of 33.03 Å obtained from crystallographic data was correlated with the d-spacing of 29.04 Å in N phase and the d-spacing of 27.13 Å in SmC phase.

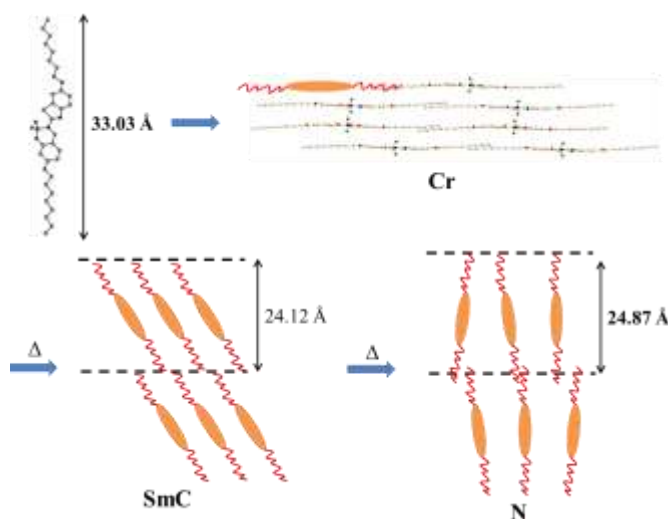


Fig. 10. The molecular arrangements proposed for boron complex **2-BF₂** ($n = 8$) in Cr, N and SmC phases. The molecular length of 33.03 Å obtained from crystallographic data was correlated with the d-spacing of 24.87 Å in N phase and the d-spacing of 24.12 Å in SmC phase.

2.5 Optical properties

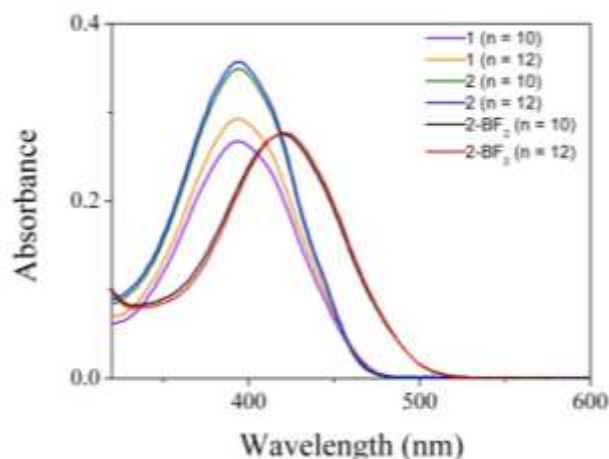
Photophysical behavior of few representative compounds **1-2** and **2-BF₂** (all $n = 10, 12$) dissolved in CH₂Cl₂ solution at room temperature are presented in **Fig. 11**. The λ_{\max} peaks of UV-vis absorptions and PL spectra for these compounds were listed in Table 8. Both UV-vis absorptions and PL emission spectra were insensitive to the carbon number of terminal alkoxy chains. The PL spectra were excited at 393 (for **1**), 394 (for **2**) and 420 nm (for **2-BF₂**). On the UV-vis spectra, a strong broad absorption peak at 393–394 nm was observed for compounds **1** and **2**, which were attributed to $\pi-\pi^*$ transitions arising from heterocyclic ring. The two UV spectra profiles for complexes **1** and **2** were almost identical due to their similar structures. For the HBO and HBT, an absorption at 320 and 332 nm, and an emission peak at 500 and 530 nm (see Table 8) was observed; the large Stokes shift was attributed to the ESIPT. In contrast, the absorption λ_{\max} peaks of complexes **2-BF₂** ($n = 10, 12$) were slightly red-shifted to 420 nm; a red-shift of $\Delta\lambda_{\max} = 26-27$ nm from those of chelating ligands **1-2** might be caused by an intramolecular electron delocalization,

leading to an extended-conjugation skeleton.

On the other hand, the PL spectra for complexes **2-BF₂** were also similar in emission peak profiles; showing one broad peak located at $\lambda_{\text{max}} = 569\text{--}571$ nm. A Stokes shift of $\Delta\lambda = 6.2\text{--}6.3 / 10^3 \text{ cm}^{-1}$, similar to those of free ligands **1-2** ($\Delta\lambda = 6.2 / 10^3 \text{ cm}^{-1}$) was obtained for boron complexes. These two boron complexes **2-BF₂** showed a red-shift emission when compared to all other similar boron complexes listed in the Table 8. This might be due to their longer molecular conjugation length.

These boron complexes adopted a typical D- π -A structure, in which terminal alkoxyphenyl group acted as the electron donor (D) and the borondifluoride moiety was as the acceptor (A).

Furthermore, the PL data indicated that the photoluminescent emissions of boron difluoride complexes were quite sensitive to the molecular structures; i.e. $\lambda_{\text{max}} = 571$ (**2-BF₂**; $n = 12$) > 541 (**III**; X = H) > 491 (**III**; X = Me) > 476 (**II**) > 433 (**HBT-BF₂**) > 408 (**HBO-BF₂**) > 368 nm (**I**). Part of the wavelength shift in PL emissions was attributed to the conjugation length. The λ_{max} of PL emissions were slightly red-shifted to 598 and 602 nm for two boron complexes (**2-BF₂**, $n = 10, 12$). However, the overall molecular planarity also played an important factor from our previous x-ray crystallographic analysis of few boron difluoride complexes. A higher fluorescence quantum yield ($\Phi_{\text{F}} = 0.44\text{--}0.47$) of boron complexes than those of free ligands ($\Phi_{\text{F}} = 0.027\text{--}0.045$) determined with anthracene ($\Phi_{\text{F}} = 0.27$ in hexane solution) as a reference dye was obtained for all three BF₂ complexes.



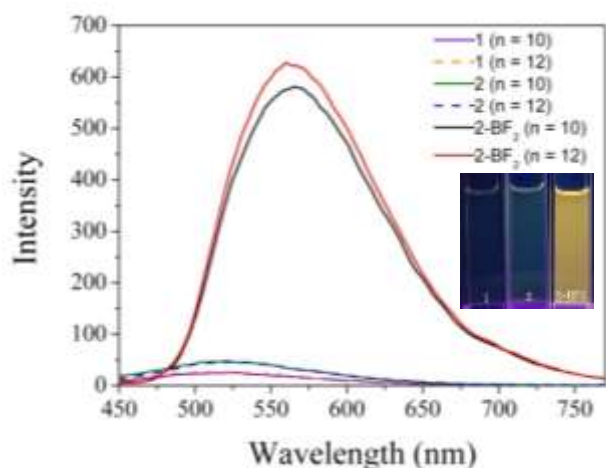


Fig. 11 UV–vis absorbance (top) and emission spectra in the CH_2Cl_2 solution (bottom) of the compounds **1-2** ($n = 10, 12$) and **2-BF₂** ($n = 10, 12$) at room temperature.

Table 8

Absorption and PL emission data^a of compounds **1-2** and **2-BF₂**.

Compds.	$\lambda_{\text{Abs}}/\text{nm}$	$\lambda_{\text{em}}/\text{nm}$	Stokes shift ($\Delta\lambda / 10^3 \text{ cm}^{-1}$)	$\Phi_{\text{F}}^{\text{b}}$
HBO ^{c,d}	320	500	11.5	0.02
HBO-BF₂	344	408	4.6	0.20
HBT ^c	332	530	11.2	0.006
HBT-BF₂	364	433	4.4	0.23
I	351	368	1.3	–
II	368	476	6.2	–
III (X = H)	393	541	6.9	–
III (X = Me)	360	491	7.4	–
1 ($n = 10$)	393 (26800)	520	6.2	0.027
1 ($n = 12$)	393 (29300)	521	6.2	0.030
2 ($n = 10$)	394 (34900)	519	6.2	0.045
2 ($n = 12$)	394 (35700)	520	6.2	0.043
2-BF₂ ($n = 10$)	420 (27600)	569/598 ^e	6.2	0.445
2-BF₂ ($n = 12$)	420 (27700)	571/602 ^e	6.3	0.473

^a: samples were measured in CH_2Cl_2 solution ($\sim 10^{-5}$ M) at rt. The samples were excited at 393 nm for **1**, 394 nm for **2** and 420 nm for **2-BF₂**.

^b: the standard is anthracene ($\Phi_{\text{F}} = 0.27$ in hexane solution).

^c: **HBO** and **HBT** is 2-(2'-hydroxyphenyl)benzoxazole and 2-(2'-hydroxyphenyl)benzothiazole.

^d: see ref.: R. Daengngern, N. Kungwan, J. of Lumi, 167 (2015) 132-139.

^e: λ_{\max} for powder sample.

3. Conclusions

Two series of benzo(thia)xazoles **1-2** and one series of borondifluoride complexes **2-BF₂** derived from benzothiazoles **2** were reported, and their mesomorphic and optical properties were investigated. The correlation between the crystal and molecular structures of compounds **2** and **2-BF₂** (all n = 8) and the formation of mesophase in such system was demonstrated. Boron complexes **2-BF₂** formed N or/and SmC phase. Boron complexes **2-BF₂** emitted a yellow-to-green emission at $\lambda_{\max} = 569\text{--}571$ nm in CH₂Cl₂, red-shifted by 50–52 nm from benzothiazoles **2**. The better polarization inherent from sulfur atom incorporated was attributed to the improved mesomorphic and luminescent behavior. To our best knowledge, this is the first mesogenic BF₂ complexes derived from benzothiazoles.

4. Experimental

4.1 Techniques

All chemicals and solvents were reagent grade from Aldrich Chemical Co., and solvents were dried by standard techniques. ¹H and ¹³C NMR spectra were measured on a Bruker DRS-500. DSC thermographs were carried out on a Mettler DSC-822 and calibrated with a pure indium sample. All phase transitions are determined by a scan rate of 10.0 °C/min. Optical polarized microscopy was carried out on Zeiss Axioplan 2 equipped with a hot stage system of Mettler FP90/FP82HT. Elemental analyses were performed on a Heraeus CHN-Rapid elemental analyzer. The powder diffraction data were collected from the Wiggie A beam line of the National Synchrotron Radiation

Research Center (NSRRC) with a wavelength of 1.3223 Å. The powder samples were charged in Lindeman capillary tubes (80 mm long x 0.01 mm thick) purchased from Charles Supper Co. with an inner diameter of 1.0 mm.

4.2 materials

The compounds of 3-alkoxyphenols, 5-alkoxy-2-nitrophenols, 2-amino-5-alkoxy phenols, 4-alkoxy-2-hydroxybenzaldehydes, 1-alkoxy-4-nitrobenzenes, 4-alkoxybenzeneamines, 5-alkoxy-2-nitro phenols and 4-alkoxy-2-hydroxybenzaldehydes were similarly prepared by literature's procedures.

4.2 6-(Dodecyloxy)benzo[d]oxazol-2-amine **3** ($n = 12$)

A solution of 2-amino-5-(dodecyloxy)phenol (2.00 g, 6.82 mmol) dissolved in 100 mL methanol was added cyanogen bromide (5.49 g, 51.83 mmol). The solution was stirred at room temperature for 4 days, and then a saturated NaHCO₃ solution was slowly added to quench the reaction. The mixture was concentrated by rotary evaporation and the mixture was extracted twice with 50 mL of ethyl acetate/H₂O (1/2). Organic layers were collected and dried over MgSO₄. The solution was concentrated under vacuum, and the products isolated as yellow solids were purified by column chromatography eluting with ethyl acetate/hexane (4/1). Yield 70%. ¹H NMR (300 MHz, *d*₆-DMSO): δ 0.85 (t, 3H, -CH₃, $J = 6.30$ Hz), 1.24–1.40 (m, 18H, -CH₂), 1.63–1.72 (m, 2H, -CH₂), 3.91 (t, 2H, -OCH₂, $J = 6.30$ Hz), 6.67 (dd, 1H, Ar-H, $^3J = 8.41$ Hz, $^4J = 2.40$ Hz), 6.98 (d, 1H, Ar-H, $J = 2.40$ Hz), 7.05 (d, 1H, Ar-H, $J = 8.41$ Hz), 7.13 (s, 2H, Ar-NH₂). ¹³C NMR (75 MHz, *d*₆-DMSO) δ 13.95, 22.12, 25.57, 28.75, 28.81, 29.04, 31.33, 68.24, 96.25, 110.23, 114.96, 136.92, 148.45, 153.56, 162.13.

4.3 (*E*)-5-(Dodecyloxy)-2-(((6-(dodecyloxy)benzo[d]oxazol-2-yl)imino)methyl)phenol **1** ($n = 12$)

A solution of 6-(dodecyloxy)benzo[d]oxazol-2-amine (0.50 g, 1.57 mmol) dissolved in 40 mL absolute ethyl alcohol was added 4-(dodecyloxy)-2-hydroxybenzaldehyde (0.48 g, 1.57 mmol). The solution was refluxed for 8 h. The solution was cooled to room temperature, and the yellow solids were filtered and collected. The products isolated as yellow powder were obtained by recrystallization from THF/MeOH. Yield 78%; mp 81.5 °C. ¹H NMR (300 MHz, CDCl₃): δ 0.86 (t, 6H, -CH₃, *J* = 6.30 Hz), 1.25–1.46 (m, 36H, -CH₂), 1.76–1.82 (m, 4H, -CH₂), 3.96–4.02 (m, 4H, -OCH₂), 6.49–6.54 (m, 2H, Ar-H), 6.90 (dd, 1H, Ar-H, ³*J* = 8.71, ⁴*J* = 2.40 Hz), 7.00 (d, 1H, Ar-H, *J* = 2.40 Hz), 7.34 (d, 1H, Ar-H, *J* = 8.41 Hz), 7.51 (d, 1H, Ar-H, *J* = 8.71 Hz), 9.22 (s, 1H, -CH=N), 12.60 (s, 1H, Ar-OH). ¹³C NMR (75 MHz, CDCl₃): δ 14.05, 22.64, 25.90, 26.02, 28.94, 29.21, 29.30, 29.35, 29.54, 29.60, 31.88, 68.57, 68.91, 96.11, 101.51, 109.21, 112.47, 113.22, 119.49, 135.36, 135.52, 150.55, 157.56, 161.55, 164.94, 165.82, 167.33. MS (HRFAB, *m/z*): calcd for [M+H]⁺: 606.4400. Found: 606.4389. Calcd for C₃₈H₅₈N₂O₄: C, 75.21; H, 9.69; N, 4.62; Found: C, 74.82; H, 9.69; N, 4.55.

4.4 (*E*)-5-(*Octyloxy*)-2-((6-(*octyloxy*)benzo[d]oxazol-2-ylimino)methyl)phenol **1** (*n* = 8)

Yellow powder; yield 78%; mp 66.5 °C. ¹H NMR (300 MHz, CDCl₃): δ 0.87 (t, 6H, -CH₃, *J* = 6.00 Hz), 1.27–1.46 (m, 20H, -CH₂), 1.74–1.82 (m, 4H, -CH₂), 3.96–4.02 (m, 4H, -OCH₂), 6.49–6.54 (m, 2H, Ar-H), 6.90 (dd, 1H, Ar-H, ³*J* = 8.71, ⁴*J* = 2.40 Hz), 7.00 (d, 1H, Ar-H, *J* = 2.40 Hz), 7.34 (d, 1H, Ar-H, *J* = 8.41 Hz), 7.51 (d, 1H, Ar-H, *J* = 8.71 Hz), 9.22 (s, 1H, -CH=N), 12.60 (s, 1H, Ar-OH). ¹³C NMR (75 MHz, CDCl₃): δ 14.07, 22.64, 25.94, 26.06, 28.97, 29.24, 29.36, 31.80, 68.61, 68.94, 96.14, 101.55, 109.25, 112.51, 113.26, 119.53, 135.39, 135.56, 150.59, 157.59, 161.58, 164.97, 165.86, 167.37. MS (HRFAB, *m/z*): calcd for [M+H]⁺: 494.3100. Found: 494.3140. Calcd for C₃₀H₄₂N₂O₄: C, 72.84; H, 8.53; N, 5.58; Found: C, 72.45; H, 8.53; N, 5.58.

4.5 (*E*)-5-(*Decyloxy*)-2-((6-(*decyloxy*)benzo[d]oxazol-2-ylimino)methyl)phenol **1** (*n* = 10)

Yellow powder; yield 82%; mp 70.6 °C. ¹H NMR (300 MHz, CDCl₃): δ 0.86 (t, 6H, -CH₃, *J* = 6.30 Hz), 1.26–1.46 (m, 28H, -CH₂), 1.76–1.82 (m, 4H, -CH₂), 3.96–4.02 (m, 4H, -OCH₂),

6.49–6.54 (m, 2H, Ar–H), 6.90 (dd, 1H, Ar–H, $^3J = 8.71$, $^4J = 2.40$ Hz), 7.00 (d, 1H, Ar–H, $J = 2.10$ Hz), 7.44 (d, 1H, Ar–H, $J = 8.71$ Hz), 7.51 (d, 1H, Ar–H, $J = 8.71$ Hz), 9.21 (s, 1H, –CH=N), 12.60 (s, 1H, Ar–OH). ^{13}C NMR (75 MHz, CDCl_3): δ 14.07, 22.66, 25.93, 26.04, 28.96, 29.23, 29.29, 29.38, 29.53, 31.88, 68.60, 68.93, 96.13, 101.54, 109.23, 112.50, 113.25, 119.51, 135.38, 135.55, 150.58, 157.58, 161.57, 164.96, 165.85, 167.36. MS (HRFAB, m/z): calcd for $[\text{M}+\text{H}]^+$: 550.3800. Found: 550.3763. Calcd for $\text{C}_{34}\text{H}_{50}\text{N}_2\text{O}_4$: C, 74.14; H, 9.15; N, 5.08; Found: C, 73.96; H, 9.221; N, 5.01.

4.6 (*E*)-5-(Tetradecyloxy)-2-((6-(tetradecyloxy)benzo[*d*]oxazol-2-ylimino)methyl)phenol **1** ($n = 14$)

Yellow powder; yield 81%; mp 86.7 °C. ^1H NMR (300 MHz, CDCl_3): δ 0.86 (t, 6H, –CH₃, $J = 6.60$ Hz), 1.25–1.46 (m, 44H, –CH₂), 1.77–1.81 (m, 4H, –CH₂), 3.96–4.03 (m, 4H, –OCH₂), 6.49–6.54 (m, 2H, Ar–H), 6.91 (dd, 1H, Ar–H, $^3J = 8.71$, $^4J = 2.40$ Hz), 7.01 (d, 1H, Ar–H, $J = 2.40$ Hz), 7.34 (d, 1H, Ar–H, $J = 8.71$ Hz), 7.51 (d, 1H, Ar–H, $J = 8.71$ Hz), 9.22 (s, 1H, –CH=N), 12.60 (s, 1H, Ar–OH). ^{13}C NMR (75 MHz, CDCl_3): δ 14.09, 22.68, 25.94, 26.05, 28.97, 29.25, 29.34, 29.58, 29.66, 31.92, 68.61, 68.95, 96.16, 101.56, 109.25, 112.52, 113.27, 119.53, 135.40, 135.56, 150.59, 157.60, 161.60, 164.98, 165.87, 167.38. MS (HRFAB, m/z): calcd for $[\text{M}+\text{H}]^+$: 662.5000. Found: 662.5024. Calcd for $\text{C}_{42}\text{H}_{66}\text{N}_2\text{O}_4$: C, 76.09; H, 10.03; N, 4.23; Found: C, 75.90; H, 9.99; N, 4.21.

4.7 (*E*)-5-(Hexadecyloxy)-2-((6-(hexadecyloxy)benzo[*d*]oxazol-2-ylimino)methyl)phenol **1** ($n = 16$)

Yellow powder; yield 82%; mp 89.6 °C. ^1H NMR (300 MHz, CDCl_3): δ 0.86 (t, 6H, –CH₃, $J = 6.30$ Hz), 1.24–1.46 (m, 52H, –CH₂), 1.76–1.82 (m, 4H, –CH₂), 3.96–4.03 (m, 4H, –OCH₂), 6.49–6.54 (m, 2H, Ar–H), 6.90 (dd, 1H, Ar–H, $^3J = 8.71$, $^4J = 2.40$ Hz), 7.01 (d, 1H, Ar–H, $J = 2.40$ Hz), 7.34 (d, 1H, Ar–H, $J = 8.41$ Hz), 7.51 (d, 1H, Ar–H, $J = 8.71$ Hz), 9.22 (s, 1H, –CH=N), 12.60 (s, 1H, Ar–OH). ^{13}C NMR (75 MHz, CDCl_3): δ 14.10, 2.68, 25.95, 26.04, 28.92, 29.00, 29.35, 29.58, 29.68, 30.33, 31.92, 68.53, 68.75, 101.09, 101.50, 105.23, 108.78, 108.96, 112.35, 116.15,

123.27, 135.20, 157.16, 164.47, 165.14, 165.37, 167.15. MS (HRFAB, m/z): calcd for $[M+H]^+$: 718.5600. Found: 718.5653. Calcd for $C_{46}H_{74}N_2O_4$: C, 76.83; H, 10.37; N, 3.90; Found: C, 76.77; H, 10.20; N, 3.89.

4.8 6-(Dodecyloxy)benzo[d]thiazol-2-amine **4** ($n = 12$)

The 2-amino-6-substituted benzothiazoles were prepared by mixing 4-(dodecyloxy)benzenamine (10.00 g, 36.04 mmol) and potassium thiocyanate (7.01 g, 72.08 mmol) in 50 ml of 96% acetic acid. To this was added drop wise, with stirring, a solution of Br_2 (1.86 mL, 36.04 mmol) in 25 ml of glacial acetic acid. After all the bromine solution was added, the mixture was stirred for another 24 h at room temperature, and NH_4OH solution was slowly added to quench the reaction. The mixture was concentrated by rotary evaporation and the mixture was extracted twice with 80 mL ethyl acetate/ H_2O (1/2). Organic layers were collected and dried over $MgSO_4$. The solution was concentrated under vacuum, and the products isolated as yellow solids were purified by column chromatography eluting with ethyl acetate/hexane (4/1). Yield 40%. 1H NMR (300 MHz, d_6 -DMSO): δ 0.85 (t, 3H, $-CH_3$, $J = 5.70$ Hz), 1.24–1.39 (m, 18H, $-CH_2$), 1.64–1.70 (m, 2H, $-CH_2$), 3.91 (t, 2H, $-OCH_2$, $J = 6.30$ Hz), 6.78 (dd, 1H, Ar-H, $^3J = 8.71$, $^4J = 2.40$ Hz), 7.18–7.22 (m, 3H, Ar-H, Ar- NH_2), 7.26 (d, 1H, Ar-H, $J = 2.40$ Hz). ^{13}C NMR (75 MHz, d_6 -DMSO): δ 13.92, 22.09, 25.52, 28.71, 28.76, 29.00, 31.29, 67.96, 106.18, 113.35, 117.99, 131.84, 146.75, 153.61, 164.65.

4.9 (E)-5-(Dodecyloxy)-2-(((6-(dodecyloxy)benzo[d]thiazol-2-yl)imino)methyl)phenol **2** ($n = 12$)

A solution of 6-(dodecyloxy)benzo[d]thiazol-2-amine (0.50 g, 1.49 mmol) dissolved in 30 mL absolute ethyl alcohol added 4-(dodecyloxy)-2-hydroxybenzaldehyde (0.46 g, 1.49 mmol). The solution was refluxed for 8 h. The solution was cooled to room temperature, and the yellow solids were filtered and collected. The products isolated as yellow powder were obtained by recrystallization from THF/MeOH. Yield 80%; mp 89.2 °C. 1H NMR (300 MHz, $CDCl_3$): δ 0.86 (t,

6H, $-\text{CH}_3$, $J = 6.30$ Hz), 1.25–1.46 (m, 36H, $-\text{CH}_2$), 1.75–1.82 (m, 4H, $-\text{CH}_2$), 3.99 (t, 4H, $-\text{OCH}_2$, $J = 6.60$ Hz), 6.49–6.53 (m, 2H, Ar-H), 7.04 (dd, 1H, Ar-H, $^3J = 8.71$, $^4J = 2.40$ Hz), 7.25 (d, 1H, Ar-H, $J = 2.40$ Hz), 7.33 (d, 1H, Ar-H, $J = 8.71$ Hz), 7.79 (d, 1H, Ar-H, $J = 9.01$ Hz), 9.04 (s, 1H, $-\text{CH}=\text{N}$), 12.63 (s, 1H, Ar-OH). ^{13}C NMR (75 MHz, CDCl_3): δ 14.12, 22.70, 25.95, 26.05, 28.99, 29.25, 29.35, 29.60, 29.65, 31.92, 68.53, 68.72, 101.47, 105.18, 108.97, 110.57, 112.31, 116.14, 123.26, 135.21, 135.48, 157.13, 164.45, 165.14, 165.35, 167.14. MS (HRFAB, m/z): calcd for $[\text{M}+\text{H}]^+$: 622.4200. Found: 622.4166. Calcd for $\text{C}_{38}\text{H}_{58}\text{N}_2\text{O}_3\text{S}$: C, 73.27; H, 9.38; N, 4.50; S, 5.15; Found: C, 73.15; H, 9.49; N, 4.44; S, 5.20.

4.10 (*E*)-5-(Octyloxy)-2-(((6-(octyloxy)benzo[d]thiazol-2-yl)imino)methyl)phenol **2** ($n = 8$)

Yellow powder; yield 82%; mp 78.4 °C. ^1H NMR (300 MHz, CDCl_3): δ 0.87 (t, 6H, $-\text{CH}_3$, $J = 6.90$ Hz), 1.27–1.45 (m, 20H, $-\text{CH}_2$), 1.73–1.84 (m, 4H, $-\text{CH}_2$), 3.98 (t, 4H, $-\text{OCH}_2$, $J = 6.60$ Hz), 6.48–6.52 (m, 2H, Ar-H), 7.03 (dd, 1H, Ar-H, $^3J = 8.71$, $^4J = 2.40$ Hz), 7.33 (d, 1H, Ar-H, $J = 8.71$ Hz), 7.78 (d, 1H, Ar-H, $J = 8.71$ Hz), 9.02 (s, 1H, $-\text{CH}=\text{N}$), 12.63 (s, 1H, Ar-OH). ^{13}C NMR (75 MHz, CDCl_3): δ 14.12, 22.68, 25.97, 26.07, 29.01, 29.26, 29.31, 29.37, 31.73, 68.53, 68.71, 101.46, 105.16, 108.96, 112.31, 116.14, 123.26, 135.21, 135.47, 145.78, 157.13, 164.45, 165.13, 165.35, 167.13. MS (HRFAB, m/z): calcd for $[\text{M}+\text{H}]^+$: 510.2900. Found: 510.2919. Calcd for $\text{C}_{30}\text{H}_{42}\text{N}_2\text{O}_3\text{S}$: C, 70.55; H, 8.29; N, 5.48; S, 6.28; Found: C, 70.49; H, 8.28; N, 5.49; S, 6.36.

4.11 (*E*)-5-(Decyloxy)-2-(((6-(decyloxy)benzo[d]thiazol-2-yl)imino)methyl)phenol **2** ($n = 10$)

Yellow powder; yield 81%; mp 87.1 °C. ^1H NMR (300 MHz, CDCl_3): δ 0.86 (t, 6H, $-\text{CH}_3$, $J = 6.90$ Hz), 1.25–1.45 (m, 28H, $-\text{CH}_2$), 1.73–1.82 (m, 4H, $-\text{CH}_2$), 3.98 (t, 4H, $-\text{OCH}_2$, $J = 6.60$ Hz), 6.48–6.52 (m, 2H, Ar-H), 7.03 (dd, 1H, Ar-H, $^3J = 9.01$, $^4J = 2.40$ Hz), 7.33 (d, 1H, Ar-H, $J = 8.41$ Hz), 7.78 (d, 1H, Ar-H, $J = 9.01$ Hz), 9.02 (s, 1H, $-\text{CH}=\text{N}$), 12.63 (s, 1H, Ar-OH). ^{13}C NMR (75 MHz, CDCl_3): δ 14.15, 22.70, 25.96, 26.06, 29.00, 29.26, 29.34, 29.41, 29.57, 31.91, 68.53, 68.70, 101.45, 105.14, 108.98, 112.30, 116.15, 123.26, 135.22, 135.47, 145.76, 157.13, 164.44, 165.14,

165.35, 167.14. MS (HRFAB, m/z): calcd for $[M+H]^+$: 566.3500. Found: 566.3535. Calcd for $C_{50}H_{42}N_2O_3S$: C, 72.04; H, 8.89; N, 4.94; S, 5.66; Found: C, 71.63; H, 8.89; N, 4.94; S, 5.72.

4.12 (*E*)-5-(Tetradecyloxy)-2-(((6-(tetradecyloxy)benzo[d]thiazol-2-yl)imino)methyl)phenol **2**
($n = 14$)

Yellow powder; yield 82%; mp 85.8 °C. 1H NMR (300 MHz, $CDCl_3$): δ 0.86 (t, 6H, $-CH_3$, $J = 6.30$ Hz), 1.24–1.46 (m, 44H, $-CH_2$), 1.75–1.82 (m, 4H, $-CH_2$), 3.99 (t, 4H, $-OCH_2$, $J = 6.30$ Hz), 6.49–6.53 (m, 2H, Ar-H), 7.04 (dd, 1H, Ar-H, $^3J = 8.71$, $^4J = 2.40$ Hz), 7.25 (d, 1H, Ar-H, $J = 2.40$ Hz), 7.34 (d, 1H, Ar-H, $J = 8.41$ Hz) 7.79 (d, 1H, Ar-H, $J = 8.71$ Hz), 9.04 (s, 1H, $-CH=N$), 12.64 (s, 1H, Ar-OH). ^{13}C NMR (75 MHz, $CDCl_3$): δ 14.12, 22.70, 25.96, 26.05, 29.00, 29.37, 29.60, 29.68, 31.93, 68.53, 68.73, 101.49, 105.20, 108.97, 112.32, 122.65, 116.15, 123.27, 135.21, 145.80, 157.14, 164.46, 165.15, 165.36, 167.15. MS (HRFAB, m/z): calcd for $[M+H]^+$: 678.4800. Found: 678.4803. Calcd for $C_{42}H_{66}N_2O_3S$: C, 74.29; H, 9.80; N, 4.13; S, 4.72; Found: C, 74.12; H, 9.84; N, 4.11; S, 4.78.

4.13 Boron complex of 7-(octyloxy)-3-(6-(octyloxy)benzo[d]thiazol-2-yl)-2,2-difluoro-2H- benzo[e][1,3,2]oxazaborinin-3-ium-2-uide **2-BF₂** ($n = 8$)

To a solution of (*E*)-5-(octyloxy)-2-(((6-(octyloxy)benzo[d]thiazol-2-yl)imino)methyl)phenol (0.4 g, 0.78 mmol) dissolved in 30 mL CH_2Cl_2 , boron trifluoride diethyl etherate (0.19 mL, 1.55 mmol) was slowly added and the mixture was refluxed for 1.5 h. The solution was concentrated and purified by column chromatography eluting with CH_2Cl_2 . The solvent was evaporated and the products, isolated as orange powders, were obtained by recrystallization from CH_2Cl_2 /hexane. Yield 30%; mp 116.1 °C. 1H NMR (500 MHz, $CDCl_3$): δ 0.87 (t, 6H, $-CH_3$, $J = 6.75$ Hz), 1.2–1.49 (m, 22H, $-CH_2$), 1.78–1.83 (m, 4H, $-CH_2$), 4.00 (t, 2H, $-OCH_2$, $J = 6.55$ Hz), 4.06 (t, 2H, $-OCH_2$, $J = 6.50$ Hz), 6.53 (sd, 1H, Ar-H, $^4J = 2.15$ Hz), 6.62 (dd, 1H, Ar-H, $^3J = 9.00$, $^4J = 2.23$ Hz), 7.08 (dd, 1H, Ar-H, $^3J = 9.00$, $^4J = 2.45$ Hz), 7.27 (sd, 1H, Ar-H, $^4J = 2.50$ Hz), 7.47 (d, 1H, Ar-H, $J = 8.90$

Hz), 7.79 (d, 1H, Ar-H, $J = 8.95$ Hz), 9.36 (s, 1H, -CH=N). ^{13}C NMR (75 MHz, CDCl_3): δ 14.13, 22.68, 25.88, 26.06, 28.76, 29.25, 29.37, 31.83, 68.76, 69.39, 101.84, 104.49, 112.99, 117.0, 123.27, 135.0, 143.65, 157.63, 158.41, 170.87. ^{19}F NMR (282.45 MHz, CDCl_3): δ -133.47 ($^{10}\text{B-F}$, 0.2 F), -133.54 ($^{11}\text{B-F}$, 0.8 F). MS (HRFAB, m/z): Calcd for $[\text{M}+\text{H}]^+$: 558.2900. Found: 558.2890. Calcd for $\text{C}_{30}\text{H}_{41}\text{BF}_2\text{N}_2\text{O}_3\text{S}$: C, 64.5; H, 7.4; N, 5.0. Found; C, 64.51; H, 7.277; N, 4.98.

4.14 Boron complex of 7-(decyloxy)-3-(6-(decyloxy)benzo[d]thiazol-2-yl)-2,2-difluoro-2H-benzo[e][1,3,2]oxaza borinin-3-ium-2-uide **2-BF₂** ($n = 10$)

Orange powders; yield 27%; mp 117.0 °C. ^1H NMR (500 MHz, CDCl_3): δ 0.87 (t, 6H, -CH₃, $J = 6.60$ Hz), 1.26–1.54 (m, 29H, -CH₂), 1.78–1.83 (m, 4H, -CH₂), 4.00 (t, 2H, -OCH₂, $J = 6.55$ Hz), 4.06 (t, 2H, -OCH₂, $J = 6.50$ Hz), 6.53 (sd, 1H, Ar-H, $^4J = 2.00$ Hz), 6.61 (dd, 1H, Ar-H, $^3J = 8.75$, $^4J = 2.25$ Hz), 7.08 (dd, 1H, Ar-H, $^3J = 8.50$, $^4J = 2.48$ Hz), 7.27 (sd, 1H, Ar-H, $^4J = 2.45$ Hz), 7.47 (d, 1H, Ar-H, $J = 8.90$ Hz), 7.79 (d, 1H, Ar-H, $J = 8.9$ Hz), 9.36 (s, 1H, -CH=N). ^{13}C NMR (75 MHz, CDCl_3): δ 14.14, 22.70, 25.87, 26.05, 28.76, 29.33, 29.58, 31.91, 68.75, 69.39, 101.85, 104.49, 109.74, 112.98, 117.0, 123.27, 135.01, 136.78, 143.65, 157.63, 158.40, 170.86. ^{19}F NMR (282.45 MHz, CDCl_3): δ -133.48 ($^{10}\text{B-F}$, 0.2 F), -133.55 ($^{11}\text{B-F}$, 0.8 F). MS (HRFAB, m/z): calcd for $[\text{M}+\text{H}]^+$: 614.3500. Found: 614.3535. Calcd for $\text{C}_{34}\text{H}_{49}\text{BF}_2\text{N}_2\text{O}_3\text{S}$: C, 66.4; H, 8.0. N, 4.6. Found: C, 66.46; H, 8.042. N, 4.53.

4.15 Boron complex of 7-(dodecyloxy)-3-(6-(dodecyloxy)benzo[d]thiazol-2-yl)-2,2-difluoro-2H-benzo[e][1,3,2] oxazaborinin-3-ium-2-uide **2-BF₂** ($n = 12$)

Orange powders; yield 25%; mp 111.0 °C. ^1H NMR (300 MHz, CDCl_3): δ 0.86 (t, 6H, -CH₃, $J = 6.60$ Hz), 1.25–1.51 (m, 35H, -CH₂), 1.75–1.85 (m, 4H, -CH₂), 4.00 (t, 2H, -OCH₂, $J = 6.56$ Hz), 4.05 (t, 2H, -OCH₂, $J = 6.56$ Hz), 6.52 (sd, 1H, Ar-H, $^4J = 2.04$ Hz), 6.60 (dd, 1H, Ar-H, $^3J = 9.00$, $^4J = 2.18$ Hz), 7.07 (dd, 1H, Ar-H, $^3J = 9.00$, $^4J = 2.43$ Hz), 7.26 (sd, 1H, Ar-H, $^4J = 2.40$ Hz), 7.46 (d, 1H, Ar-H, $J = 8.90$ Hz), 7.78 (d, 1H, Ar-H, $J = 8.9$ Hz), 9.35 (s, 1H, -CH=N). ^{13}C NMR (75

MHz, CDCl₃): δ 14.14, 22.71, 25.87, 26.05, 28.76, 29.21, 29.28, 29.36, 29.53, 29.65, 31.93, 68.75, 69.38, 101.84, 104.49, 109.73, 112.95, 116.98, 123.27, 135.01, 136.75, 143.65, 157.63, 158.39, 164.41, 170.84. ¹⁹F NMR (282.45 MHz, CDCl₃): δ -133.45 (¹⁰B-F, 0.2 F), -133.53 (¹¹B-F, 0.8 F).. MS (HRFAB, m/z): calcd for [M+H]⁺: 670.4200. Found: 670.4150. Calcd for C₃₈H₅₇BF₂N₂O₃S: C, 68.0; H, 8.6; N, 4.2; Found: C, 67.74; H, 8.741; N, 4.07.

Acknowledgements

We thank the Ministry of Science and Technology, Taiwan, ROC (MOST 107-2113-M-008-009) in generous support of this work. Also we deeply appreciated Prof. Hwo-Shuenn Sheu for performing powder XRD experiments at the National Synchrotron Radiation Research Center.

References

- [1] H. Ye, D.H. Kim, X. Chen, A.S.D. Sandanayaka, J.U. Kim, E. Zaborova, G. Canard, Y. Tsuchiya, E.Y. Choi, J.W. Wu, F. Fages, J.L. Bredas, A. D'Aleo, J. C. Ribierre, C. Adachi, *Chem. Mater.* 30 (2018) 6702–6719.
- [2] A.L. Johnson. *Annu. Rep. Prog. Chem., Sect. A Inorg. Chem.* 108 (2012) 61–84.
- [3] F. Wang, C.A. DeRosa, M.L. Daly, D. Song, M. Sabat, C.L. Fraser, *Mater. Chem. Front.* 1 (2017) 1866–1874.
- [4] A. D'Aleo, D. Gachet, V. Heresanu, M. Giorgi, F. Fages, *Chem. Eur. J.* 18 (2012) 12764–12772.
- [5] T.L. Wu, M.J. Huang, C.C. Lin, P.Y. Huang, T.Y. Chou, R.W. Chen-Cheng, H.W. Lin, R.S. Liu, C.H. Cheng, *Nature Photonics* (2018) <https://doi.org/10.1038/s41566-018-0112-9>.
- [6] A. D'Aleo, M. H. Sazzad, D. H. Kim, E. Y. Choi, J. W. Wu, G. Canard, F. Fages, J.C. Ribierre, C. Adachi, *Chem. Commun.* 53 (2017) 7003–7006.
- [7] K. Tanaka, Y. Chujo, *NPG Asia Materials* 7 (2015) e223; doi:10.1038/am.2015.118.

- [8] G. Canard, M. Ponce-Vargas, D. Jacquemin, B.L. Guennic, A. Felouat, M. Rivoal, E. Zaborova, A. D'Aleo, F. Fages, *RSC Adv.* 7 (2017) 10132–10142.
- [9] E. Kim, A. Felouat, E. Zaborova, J.C. Ribierre, J.W. Wu, S. Senatore, C. Matthews, P.F. Lenne, C. Baffert, A. Karapetyan, M. Giorgi, D. Jacquemin, M. Ponce-Vargas, B.L. Guennic, Frédéric Fages, A. D'Aléo, *Org. Biomol Chem.* 14 (2016) 1311–1324.
- [10] M. Rivoal, E. Zaborova, G. Canard, A. D'Aleo, F. Fages, *New J. Chem.* 40 (2016) 1297–1305.
- [11] S.A. Tikhonov, V.I. Vovna, N.A. Gelfand, I.S. Osmushko, E.V. Fedorenko, A.G. Mirochnik, *J. Phys. Chem. A* 120 (2016) 7361–7369.
- [12] Q. Tang, W. Si, C. Huang, K. Ding, W. Huang, P. Chen, Q. Zhang, X. Dong, *J. Mater. Chem. B* 5 (2017) 1566–1573.
- [13] W. Fang, Y. Zhang, G. Zhang, L. Kong, L. Yanga, J. Yang, *CrystEngComm.* 19 (2017) 1294–1303.
- [14] K. Benelhadj, J. Massue, G. Ulrich, *New J. Chem.* 40 (2016) 5877–5884.
- [15] S. Maity, S. Pal, S. Sardar, N. Sepay, H. Parvej, J. Chakraborty, U.C. Halder, *RSC Adv.* 6 (2016) 112175–112183.
- [16] R. Tan, Q. Lin, Y. Wen, S. Xiao, S. Wang, R. Zhanga, T. Yi, *CrystEngComm.* 17 (2015) 6674–6680.
- [17] S. M. Barbon, J.T. Price, P.A. Reinkeluers, J.B. Gilroy, *Inorg. Chem.* 53 (2014) 10585–10593.
- [18] H. Kang, Y. Si, Y. Liu, X. Zhang, W. Zhang, Y. Zhao, B. Yang, Y. Liu, Z. Liu, *J. Phys. Chem. A.* 122 (2018) 5574–5579.
- [19] A. Gut, L. Lapok, D. Jamroz, A. Gorski, J. SolarSKI, M. Nowakowska, *New J. Chem.*, 41 (2017) 12110–12122.
- [20] W. Ren, H. Xiang, C. Peng, Z. Musha, J. Chen, X. Li, R. Huang, Y. Hu, *RSC Adv.* 8 (2018) 5542–5549.
- [21] R.R. Maar, S.M. Barbon, N. Sharma, H. Groom, L.G. Luyt, J. B. Gilroy, *Chem. Eur. J.* 21 (2015) 15589–15599.

- [22] D.R. Vinayakumara, K. Swamynathan, S. Kumar, A.V. Adhikari, *New J. Chem.* 43 (2019) 7099–7108.
- [23] I. Sanchez, A. Fernandez–Lodeiro, E. Oliveira, J.A. Campo, M.R. Torres, M. Cano, C. Lodeiro, *Dyes and Pigment* 135 (2016) 184–200.
- [24] I. Sanchez, C. Nunez, J.A. Campo, M.R. Torres, M. Cano, C. Lodeiro, *J. Mater. Chem. C*, 2 (2014) 9653–9665.
- [25] M. Chapran, E. Angioni, N.J. Findlay, B. Breig, V. Cherpak, P. Stakhira, T. Tuttle, D. Volyniuk, J. V. Grazulevicius, Y.A. Nastishin, O.D. Lavrentovich, P.J. Skabara, *ACS Appl. Mater. Interfaces* 9 (2017) 4750–4757.
- [26] Y.W. Chen, Y.C. Lin, H.M. Kuo, C.K. Lai, *J. Mater. Chem. C*, 5 (2017) 5465–5477.
- [27] D. Rohde, C.Y. Yan, L.J. Wan, *Langmuir* 22 (2006) 4750–4757.
- [28] Y. Sun, D. Rohde, Y. Liu, L. Wan, Y. Wang, W. Wu, C. Di, G. Yua, D. Zhu, *J. Mater. Chem.*, 16 (2006) 4499–4503.
- [29] M. Ishida, T. Omagari, R. Hirosawa, K. Jono, Y.M. Sung, Y. Yasutake, H. Uno, M. Toganoh, H. Nakanotani, S. Fukatsu, D. Kim, H. Furuta, *Angew. Chem. Int. Ed.* 55 (2016) 1–6.
- [30] S. Ogawa, M. Morikawa, G. Juhasza, N. Kimizuka, *RSC Adv.* 5 (2015) 60373–60379.
- [31] J. Zhao, J. Peng, P. Chen, H. Wang, P. Xue, R. Lu, *Dyes and Pigments* 149 (2018) 276–283.
- [32] W. Duan, Q. Liu, Y. Huo, J. Cui, S. Gong, Z. Liu, *Org. Biomol. Chem.* 16 (2018) 4977–4984.
- [33] E.V. Fedorenko, A.G. Mirochnik, A. Y. Beloliptsev, *J. of Luminescence* 196 (2018) 316–325.
- [34] J. Zhao, J. Peng, P. Chen, H. Wang, P. Xue, R. Lu, *Dyes and Pigments* 149 (2018) 276–283.
- [35] R. Yoshii, A. Hirose, K. Tanaka, Y. Chujo, *Chem. Eur. J* 20 (2014) 8320–8324.
- [36] Z. Zhang, Z. Wu, J. Sun, P. Xue, R. Lu, *RSC Adv.* 6 (2016) 43755–43766.
- [37] H. Gao, D. Xu, Y. Wang, C. Zhang, Y. Yang, X. Liu, A. Han, Y. Wang, *Dyes and Pigment* 150 (2018) 165–173.
- [38] J. Zhao, J. Peng, P. Chen, H. Wang, P. Xue, R. Lu, *Dyes and Pigment* 149 (2018) 276–283.

- [39] H. Gao, D. Xu, X. Liua, A. Hana, L. Zhou, C. Zhang, Z. Li, J. Dang, *Dyes and Pigment* 139 (2017) 157–165.
- [40] Y.J. Shiu, Y.C. Cheng, W.L. Tsai, C.C. Wu, C.T. Chao, C.W. Lu, Y. Chi, Y.T. Chen, S.H. Liu, P.T. Chou, *Angew. Chem. Int. Ed.* 55 (2016) 3017–3021.
- [41] P.J. Brothers, *Inorg. Chem.* 50 (2011) 12374–12386.
- [42] S. Madhu, M. Ravikanth, *Inorg. Chem.* 51 (2012) 4285–4292.
- [43] M.J. Kwak, Y. Kim, *Bull. Korean Chem. Soc.* 30 (2009) 2865–2866.
- [44] D. Suresh, C.S.B. Gomes, P.S. Lopes, C.A. Figueira, B. Ferreira, P.T. Gomes, R.E. Di Paolo, A.L. MaAanita, M.T. Duarte, A. Charas, J. Morgado, D. Vila-ViAosa, M.J.Calhorda, *Chem. Eur. J.* 21 (2015) 9133–9149.
- [45] R.K. Gill¹, Ravindra K. Rawal¹, J. Bariwal¹, *Arch. Pharm. Chem. Life Sci.* 348 (2015) 155–178.
- [46] R.K. Gill¹, R.K. Rawal, J. Bariwal¹, *Arch. Pharm. Chem. Life Sci.* 348 (2015) 1–24.
- [47] L. Fan, L. Wu, M. Ke, *J. Chem. Res.* 39 (2015) 442–444.
- [48] X. Wang, Q. Liu, Hui Y.Z. Liu, M. Yao, Q. Zhang, S. Gong, W. He, *Chem. Commun.* 51 (2015) 7497–7500.
- [49] P. Gong, H. Yang, J. Sun, Z. Zhang, J. Sun, P. Xue, R. Lu, *J. Mater. Chem.* 3 (2015) 10302–10308.
- [50] Y.W. Chen, G.H. Lee, C.K. Lai, *Dalton Trans.* 46 (2017) 12274–12283.
- [51] Z.Y. Lei, G.H. Lee, C.K. Lai, *J. Mol. Liq.* 260 (2018) 44–56.
- [52] T. Ghosh, M. Lehmann, *J. Mater. Chem.* 5 (2017) 12308–12337.

Highlights

- Borondifluoride complexes exhibited smectic or/and nematic phases, also emitting yellow-to-green light.
- Two crystallographic structures were correlated with mesophase observed.
- The first mesogenic borondifluoride complexes derived from benzothiazazole
- The bonding preference of borondifluoride moiety to chelating N, O atoms with crystallographic data supported.

Journal Pre-proof